


Cite this: *Chem. Sci.*, 2021, 12, 8746 All publication charges for this article have been paid for by the Royal Society of ChemistryReceived 20th March 2021  
Accepted 13th May 2021

DOI: 10.1039/d1sc01611c

rsc.li/chemical-science

# Helix-mediated over 1 nm-range chirality recognition by ligand-to-ligand interactions of dinuclear helicates†

Natsumi Suko, Hideki Itamoto, Yoshinori Okayasu, Naoya Okura  
and Junpei Yuasa \*

Long-range chirality recognition between the two chiral guest ligands can be tuned based on the helix distances ( $d_{L_n-L_n} = 11.5$  and  $14.0$  Å) of bis-diketonate bridged dinuclear lanthanide complexes (**2Th** and **3Th**, respectively) used as mediators. Both **2Th** and **3Th** form one-dimensional (1D) helical structures upon terminal binding of two chiral guest co-ligands ( $L^R$  or  $L^S$ ). Long-range chiral self-recognition is achieved in self-assembly of **2Th** with  $L^R$  and  $L^S$  to preferentially form homochiral assemblies, **2Th**- $L^R \cdot L^R$  and **2Th**- $L^S \cdot L^S$ , whereas there is no direct molecular interaction between the two guest ligands at the terminal edges. X-ray crystal structure analysis and density functional theory studies reveal that long-range chiral recognition is achieved by terminal ligand-to-ligand interactions between the bis-diketonate ligands and chiral guest co-ligands. Conversely, in self-assembly of **3Th** with a longer helix length, statistical binding of  $L^R$  and  $L^S$  occurs, forming heterochiral (**3Th**- $L^R \cdot L^S$ ) and homochiral (**3Th**- $L^R \cdot L^R$  and **3Th**- $L^S \cdot L^S$ ) assemblies in an almost 1 : 1 ratio. When phenyl side arms of the chiral guest co-ligands are replaced by isopropyl groups ( $L^{iR}$  and  $L^{iS}$ ), chiral self-recognition is also achieved in the self-assembly process of **3Th** with the longer helix length to generate homochiral (**3Th**- $L^{iR} \cdot L^{iR}$  and **3Th**- $L^{iS} \cdot L^{iS}$ ) assemblies as the favored products. Thus, subtle modification of the chiral guests is capable of achieving over 1.4 nm-range chirality recognition.

## Introduction

Molecular recognition has an important role in chemistry. High-fidelity molecular recognition is typically achieved by short-range direct intermolecular contact that enables recognition of one molecule from another through noncovalent interactions.<sup>1</sup> Conversely, long-range molecular recognition is inherently important for understanding how molecular information is recognized and transferred across long distances in supramolecular systems, even without direct intermolecular interactions.<sup>2</sup> In this context, long-range molecular recognition is particularly challenging for enantiomers that have the same size and shape, with their only distinguishing feature being the spatial orientations of certain groups.<sup>3–9</sup> Such interactions have a pivotal role in various chemical and biological phenomena.

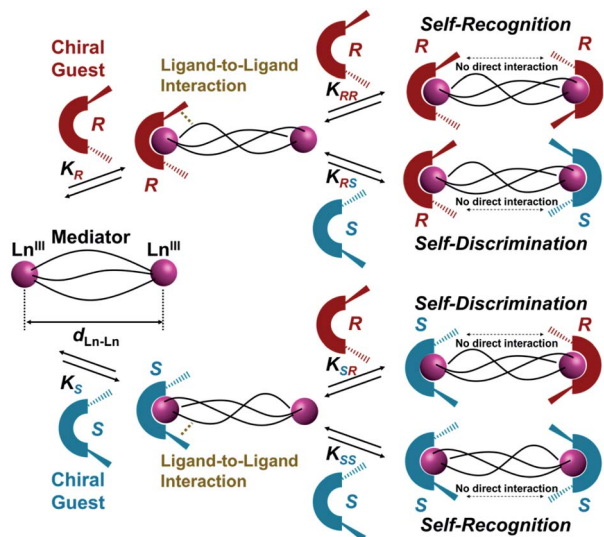
Herein, we report helix-length dependent over 1 nm-range chiral recognition by terminal binding of two chiral guest ligands across a one-dimensional (1D) helix. A helix is intrinsically chiral with either *P*- or *M*-helicity, where the preferred

helicity is induced by local chirality at the terminal edges. Hence, a helix is a prototypical motif that can mediate terminal chiral information across long distances.<sup>10</sup> In particular, a dinuclear helicate is a smart platform for investigating long-range chiral recognition because the helix distance can be tuned by adjusting the number of spacer units immobilized in bridging ligands.<sup>11–17</sup> However, most transition metal-based dinuclear helicates (such as  $M_2L_3$ ) are coordinatively saturated, therefore guest ligands are not expected to have any access. Conversely, lanthanide-based dinuclear helicates (such as  $Ln_2L_3$ ) are often coordinatively unsaturated because of the wide range of coordination numbers ( $n \geq 8$ ) of lanthanide(III) ions,<sup>12,13</sup> which enable sequential interactions with chiral co-ligands. In this context, we have extensively developed ternary lanthanide self-assembly systems comprising  $\beta$ -diketonate ligands and chiral co-ligands, which revealed that the attractive ligand-to-ligand interactions between  $\beta$ -diketonate ligands and chiral co-ligands give rise to overall chirality in the final self-assembled molecule.<sup>18</sup> Such ligand-to-ligand interactions would be suitable for transfer of molecular chirality information across long distances. Scheme 1 illustrates helix-mediated long-range chirality recognition using the ligand-to-ligand interaction approach, where there is no direct molecular interaction between two chiral ligands at the terminal edges. Herein, an initial chiral ligand binding induces *P*- or *M*-helicity of

Department of Applied Chemistry, Tokyo University of Science, 1-3, Kagurazaka, Shinjuku-ku, Tokyo 162-8601, Japan. E-mail: yuasaj@rs.tus.ac.jp

† Electronic supplementary information (ESI) available: Additional experimental details and additional data. CCDC 2036830. For ESI and crystallographic data in CIF or other electronic format see DOI: 10.1039/d1sc01611c





**Scheme 1** Helix-mediated long-range chirality recognition: chiral self-recognition is favored when  $2K_{RR} = 2K_{SS} > K_{(\text{hetero})}$ . Conversely, chiral self-discrimination will be predominant when  $2K_{RR} = 2K_{SS} < K_{(\text{hetero})}$ . Alternatively, statistical binding will occur when  $2K_{RR} = 2K_{SS} = K_{(\text{hetero})}$ . Here,  $K_{(\text{hetero})} = K_{RS} + K_{SR} = 2K_{RS} = 2K_{SR}$ .

a helicate (mediator) through ligand-to-ligand interactions at the terminal edge. When the resulting initial helicate interacts preferably with the second ligand of the same chirality ( $2K_{RR} = 2K_{SS} > K_{(\text{hetero})}$ ), chiral self-recognition takes place, forming homochiral assemblies. Here,  $K_{(\text{hetero})} = K_{RS} + K_{SR} = 2K_{RS} = 2K_{SR}$  (since  $K_{RS} = K_{SR}$ ). Conversely, chiral self-discrimination occurs when the second ligand binding prefers the opposite chirality ( $2K_{RR} = 2K_{SS} < K_{(\text{hetero})}$ ) to form heterochiral assemblies. Alternatively, when the initial helicates have no sufficient energy bias to distinguish the same and opposite chirality in the second binding event ( $2K_{RR} = 2K_{SS} = K_{(\text{hetero})}$ ), statistical binding of both enantiomers takes place. In this study, we show that chirality recognition of two chiral guest co-ligands ( $L^{(R \text{ or } S)}$ ) is highly sensitive to the helix length of the mediator, where a shorter helix ( $d_{\text{Ln-Ln}} = 11.5 \text{ \AA}$ , **2Th**) causes chiral self-recognition and a longer helix ( $d_{\text{Ln-Ln}} = 14.0 \text{ \AA}$ , **3Th**) results in statistical binding. Conversely, subtle modification of the chiral guest ligands ( $L^{(R \text{ or } S)} \rightarrow L'^{(R \text{ or } S)}$ ) enables even the longer helix ( $d_{\text{Ln-Ln}} = 14.0 \text{ \AA}$ , **3Th**) to demonstrate chiral self-recognition. Thus, the present findings provide valuable insights for unravelling the principles of molecular recognition and transfer across long distances in supramolecular systems.

## Results and discussion

### X-ray structure of dinuclear helicates

For the chirality mediator, we used selected dinuclear lanthanide complexes (**2Th** and **3Th**) having two and three thiophene spacer units, respectively, which were synthesized by reacting the corresponding bis-diketone ligands ( $L_2$  and  $L_3$ , respectively) and europium acetate in a 3 : 2 stoichiometry (Fig. S1–S3†).<sup>13b</sup> In this context, Yan *et al.* successfully revealed the helix structure of dinuclear lanthanide complexes with the bis-diketone

ligands.<sup>13b</sup> Both **2Th** and **3Th** formed 1D helical assemblies upon terminal binding of two chiral guest co-ligands [ $L^{(R \text{ or } S)}$  or  $L'^{(R \text{ or } S)}$ ] (*vide infra*).<sup>19,20</sup> Among the series of helicate assemblies, we successfully grew crystals suitable for X-ray analysis by slow evaporation of an acetone solution containing **2Th** with the presence of 2 equiv. of a racemic mixture of the chiral guest co-ligands ( $L^R$  and  $L^S$ ) having phenyl side arms. The X-ray structure analysis (Fig. 1) revealed that the both terminal Eu<sup>III</sup> ions of **2Th** were occupied by chiral guest co-ligands of the same chirality to afford homochiral assemblies, **2Th**- $L^R \cdot L^R$  and **2Th**- $L^S \cdot L^S$ , which

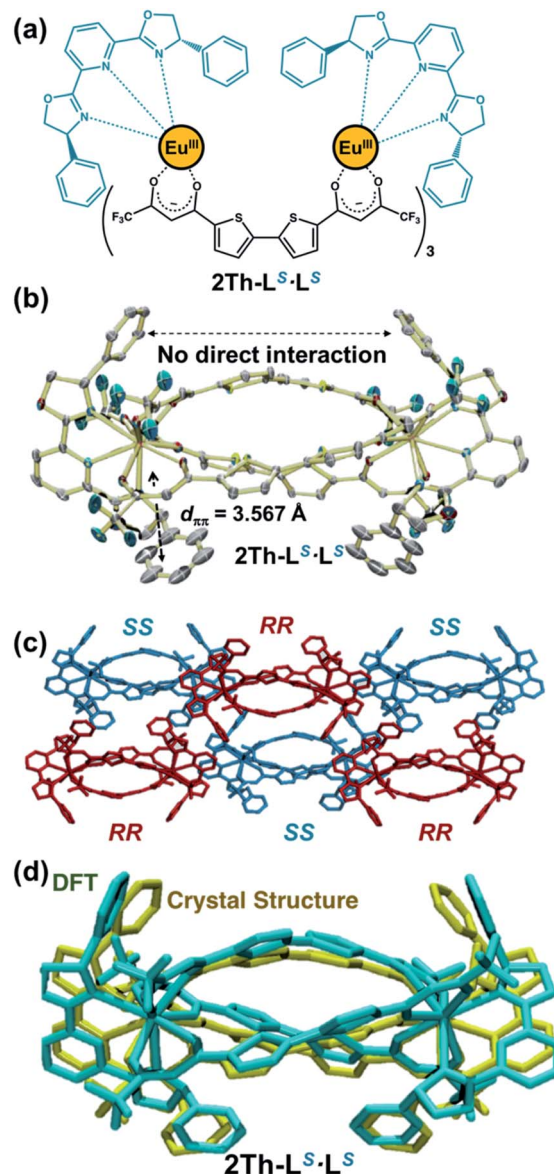


**Fig. 1** (a) Chemical structure, (b) X-ray crystal structure (ORTEP view, 50% probability) of **2Th**- $L^S \cdot L^S$  (CCDC 2036830†). (c) Crystal packing diagrams of the crystal structures of **2Th**- $L^R \cdot L^R$  (red) and **2Th**- $L^S \cdot L^S$  (blue). (d) Overlapping image of X-ray crystal structure (yellow) of **2Th**- $L^S \cdot L^S$  and optimized structure [DFT/CAM-B3LYP/def2SVP (C H N O S F)/def2TZVPP (La)] of **2Th**- $L^S \cdot L^S$ , where the Eu atoms were replaced by La atoms. Hydrogen atoms are omitted for clarity. One of the disordered structures was shown for clarity (Fig. S5†).



arranged alternatively in the crystal packing diagram (Fig. 1c). These results indicate that **2Th** with chiral guest co-ligands favored ligand chiral self-recognition over chiral self-discrimination and statistical binding. Helical structures were found in the thiophene spacer units, *i.e.*, *P*-helicity for **2Th**- $L^R \cdot L^R$  and *M*-helicity for **2Th**- $L^S \cdot L^S$  (Fig. 1c), whose helicity was induced by ligand-to-ligand interactions between the chiral guest co-ligands and the diketonate ligand units.<sup>18</sup> While no direct interaction between the two chiral ligands at the terminal edges was detected, intra-complex  $\pi$ - $\pi$  stacking ( $d_{\pi-\pi} = 3.567$  Å) was indicated between the phenyl rings of  $L^S$  and the  $\beta$ -diketonate plane (Fig. 1b). Notably, the optimized structure of **2Th**- $L^S \cdot L^S$  calculated by density functional theory (DFT) [DFT/CAM-B3LYP/def2SVP (C H N O S F)/def2TZVPP (La)] reproduced the crystal structure well (Fig. 1d and Table S1†).<sup>21</sup> Therefore, rational structural modelling of the other helicates, such as **3Th** with a flexible longer thiophene chain length that is not suitable for crystal growth, would be also possible with appropriate use of DFT calculations (*vide infra*).

### Allosteric effects on formation of dinuclear helicates

Next, we used circular dichroism (CD) spectroscopy to investigate the helicate formation of **2Th** and **3Th** through the terminal binding of chiral guest co-ligands [ $L^{(R \text{ or } S)}$  and  $L'^{(R \text{ or } S)}$ ] in solution.<sup>22–24</sup> Upon addition of the chiral guest co-ligand, **2Th** and **3Th** began to show biphasic (splitting) CD spectra with intense CD signals, whereas neither **2Th** nor **3Th** themselves exhibited CD (Fig. 2a and S5–S8†). Conversely, no notable UV-vis absorption spectral changes were observed because of the

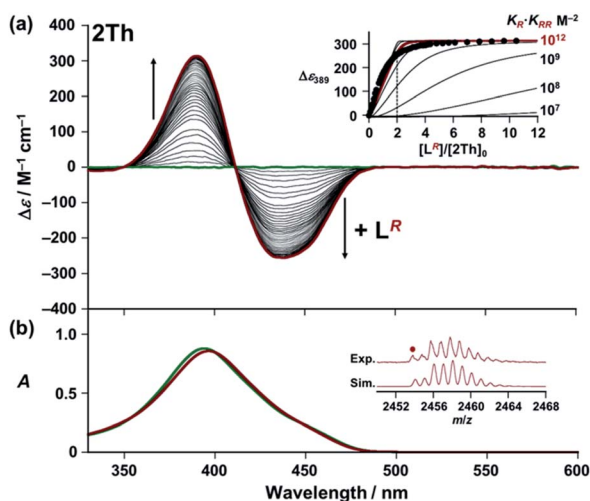
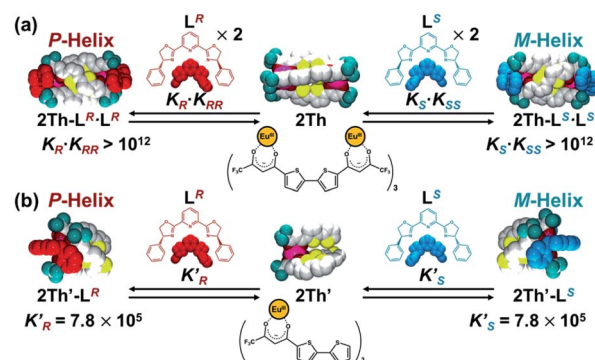


Fig. 2 (a) CD and (b) UV-vis absorption spectra of **2Th** ( $6.9 \times 10^{-6}$  M) in the presence of  $L^R$  [0 (green line) –  $7.2 \times 10^{-5}$  M (red line)] in acetone at 298 K. (Insets) (a) Plot of  $\Delta\epsilon$  at 389 nm versus  $[L^R]/[2Th]_0$ . Simulated curves were obtained based on the consecutive binding model ( $K_{RR} \gg K_R$ ):  $[L^R] = (\alpha/(K_R \cdot K_{RR}(1 - \alpha))^{0.5} + 2\alpha[2Th]_0)$ , using  $K_R \cdot K_{RR} = 10^7 - 10^{14}$  M<sup>-2</sup>. Here,  $[2Th]_0$  denotes the initial concentration of **2Th**, and  $\alpha = [2Th \cdot L^R \cdot L^R]/[2Th]_0$ . (b) Negative ESI mass spectrum of **2Th** in the presence of  $L^R$  in acetone with the calculated isotopic distributions for  $\{(\text{Eu})_2(\text{L}_2\text{-2H})_3(\text{L}^R)_2 + \text{CH}_3\text{COCH}_3 + 2\text{H}_2\text{O}\}$ . For ESI mass spectrum in the whole region (Fig. S9†).

lack of absorption by the chiral guest co-ligand ( $L^R$ ) in this region (Fig. 2b and ESI Fig. S5–S8†). A titration plot was obtained by plotting  $\Delta\epsilon$  at 389 nm against the molar ratio of **2Th** and the chiral guest co-ligand ( $[L^R]/[2Th]_0$ ), which exhibited saturation at approximately  $[L^R]/[2Th]_0 = 2.0$  (Fig. 2a inset). Subtle difference between the experimental titration curve and the theoretical one around  $[L^R]/[2Th]_0 = 2.0$  (as well as less defined saturation point) should be ascribed to a minor contribution of the mono-coordinated species (**2Th**- $L^R$ ). This result indicates a 1 : 2 binding mode between **2Th** and  $L^R$  (Scheme 2a and Fig. S5–S8†) as confirmed by the X-ray structure (*vide supra*, Fig. 1b). The **2Th**- $L^R \cdot L^R$  assembly was also analyzed by ESI mass spectrometry of **2Th** with  $L^R$  in acetone solution (Fig. 2b inset).<sup>25</sup>

Next, by using <sup>19</sup>F NMR spectroscopy, we investigated whether the two chiral guest co-ligands ( $L^R$ ) associate with **2Th** sequentially or continuously in terms of allosteric effects.<sup>26,27</sup> If the second binding constant is larger than the initial binding constant ( $K_{RR} \geq K_R$ ), continuous association of the two guest co-ligands ( $L^R$ ) to **2Th** will occur to yield the final assembly of **2Th**- $L^R \cdot L^R$  in a formally single step. Conversely when the second binding constant is comparable with the initial binding constant ( $K_{RR} \leq K_R$ ), association of  $L^R$  to **2Th** will occur sequentially through the mono-coordinated species (**2Th**- $L^R$ ). Upon addition of 2 equiv. of  $L^R$  to **2Th**, a single <sup>19</sup>F NMR signal at –83.7 ppm assigned to **2Th** (itself) split into three signals at –78.3, –85.2, and –85.4 ppm (Fig. 3c to a). Since the original **2Th** has a threefold axis, the terminal CF<sub>3</sub> groups are in the same chemical environment (Fig. 3c left).<sup>18a</sup> However, the terminal binding of the chiral guest co-ligands removes this threefold axis and places the three CF<sub>3</sub> groups in different chemical environments (Fig. 3a left). Thus, the observed <sup>19</sup>F NMR signal split, clearly suggested the formation of a helical structure of **2Th**- $L^R \cdot L^R$  based on terminal binding of the two guest co-ligands ( $L^R$ ) to **2Th** (Fig. S5–S8†). Conversely when addition of 1 eq. of  $L^R$  into **2Th** in acetone-*d*<sub>6</sub>, <sup>19</sup>F NMR signals corresponding to **2Th** (green circle) and **2Th**- $L^R \cdot L^R$  (red



Scheme 2 Self-assembly formation of (a) **2Th** and (b) **2Th'** with  $L^R$  (left) and that with  $L^S$  (right). Here,  $K_R$  denotes the binding constant between **2Th** and  $L^R$  to form **2Th**- $L^R$ , and  $K_{RR}$  means the binding constant between **2Th**- $L^R$  and  $L^R$  to generate the final assembly **2Th**- $L^R \cdot L^R$ . Conversely,  $K'_R$  denotes the binding constant between **2Th'** and  $L^R$  to form **2Th'**- $L^R$ .



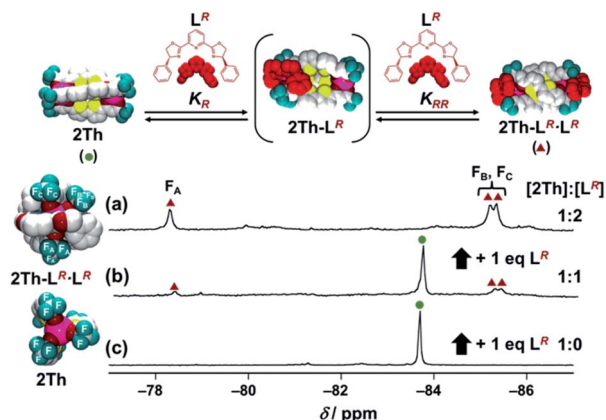


Fig. 3  $^{19}\text{F}$  NMR spectra of  $2\text{Th}$  (c) in the absence and presence of (b) 1 eq. and (a) 2 eq. of  $\text{L}^R$  in acetone- $d_6$  at 298 K. Left figures show the optimized structures of  $2\text{Th-L}^R\cdot\text{L}^R$  and  $2\text{Th}$  [DFT/CAM-B3LYP/def2SVP (C H N O S F)/def2TZVPP (La)].

triangles) were observed, while that corresponding to the mono-coordinated species ( $2\text{Th-L}^R$ ) was not detected (Fig. 3b). Further addition of  $\text{L}^R$  (2 eq.) resulted in development of  $^{19}\text{F}$  NMR signals due to  $2\text{Th-L}^R\cdot\text{L}^R$  (red triangles), where the signals corresponding to  $2\text{Th}$  (green circle) were completely disappeared (*vide supra*, Fig. 3a). Such observation suggested the continuous binding model.

With these results in hand, we rationalized the above CD titration plot (Fig. 2a inset) based on the theoretical titration curve based on the continuous binding model. Since binding between  $2\text{Th}$  and  $\text{L}^R$  is almost stoichiometric judging from the titration curve (Fig. 2a inset), the binding constant ( $K_R\cdot K_{RR}$ ) could not be determined accurately. Conversely, the theoretical titration curve suggested that the observed stoichiometric binding agreed with the binding constant at least larger than  $10^{12}\text{ M}^{-2}$  ( $K_R\cdot K_{RR} > 10^{12}\text{ M}^{-2}$ , red line in Fig. 2a inset). For further verification on the allosteric effects, we prepared a mononuclear complex  $2\text{Th}'$  and a 1 : 1 binding constant ( $K'_R$ ) with  $\text{L}^R$  was determined to be  $(7.2 \pm 0.7) \times 10^5\text{ M}^{-1}$  from a CD titration experiment of  $2\text{Th}'$  with  $\text{L}^R$  (Scheme 2b and Fig. S8†). Since the twice value of the resulting 1 : 1 binding constant ( $K'_R$ ) between  $2\text{Th}'$  and  $\text{L}^R$  is probably nearly equal to the initial binding constant ( $K_R$ ) between  $2\text{Th}$  and  $\text{L}^R$  ( $2K'_R \approx K_R$ ), the second binding constant ( $K_{RR}$ ) should be larger than  $6.9 \times 10^5\text{ M}^{-1}$  ( $K_{RR} > 6.9 \times 10^5\text{ M}^{-1}$ ). Although it could not be concluded whether binding between  $2\text{Th}$  and  $\text{L}^R$  follows the continuous binding model based on the estimated binding constants, the determined  $4K_{RR}/K_R$  value ( $4K_{RR}/K_R > 1.9$ ) suggested the allosteric effect in the present system. The observed allosteric effect could result from the initial binding event, which causes a conformational change of the helicate suitable for the second binding of the chiral co-ligand with the same chirality. The initial and the second binding energy ( $E_R^{(1)}$  and  $E_{RR}^{(2)}$ , respectively) were estimated from the optimized structures of  $\text{L}^R$ ,  $2\text{Th}$ ,  $2\text{Th-L}^R$ , and  $2\text{Th-L}^R\cdot\text{L}^R$  [DFT/CAM-B3LYP/def2SVP (C H N O S F)/def2TZVPP (La)], where the second binding energy ( $E_{RR}^{(2)}$ ) is  $7.66\text{ kcal mol}^{-1}$  larger than that of the initial binding energy

Table 1 Initial and second binding constants ( $K_R$  and  $K_{RR}$ ), binding energy ( $E_R^{(1)}$  and  $E_{RR}^{(2)}$ ) in self-assembly formation of  $2\text{Th}$  with  $\text{L}^R$

$K_R^a$ ( $\text{M}^{-1}$ )	$K_{RR}^b$ ( $\text{M}^{-1}$ )	$E_R^{(1)c}$ ( $\text{kcal mol}^{-1}$ )	$E_{RR}^{(2)c}$ ( $\text{kcal mol}^{-1}$ )
$1.4 \times 10^6$	$>6.9 \times 10^5$	36.54	44.20

<sup>a</sup> Determined from the titration experiments of  $2\text{Th}'$  with chiral guest co-ligands. <sup>b</sup> Determined from the titration experiments of  $2\text{Th}'$  and  $2\text{Th}$  with the chiral guest co-ligands. <sup>c</sup> Determined from the optimized structures of  $\text{L}^R$ ,  $2\text{Th}$ ,  $2\text{Th-L}^R$ , and  $2\text{Th-L}^R\cdot\text{L}^R$  [DFT/CAM-B3LYP/def2SVP (C H N O S F)/def2TZVPP (La)].

( $E_R^{(1)}$ ) (Table 1), which agreed with the experimentally observed allosteric effect.

### A DFT prediction on long-range chirality recognition

The biphasic CD spectra of  $2\text{Th-L}^R\cdot\text{L}^R$  and  $2\text{Th-L}^S\cdot\text{L}^S$  (Fig. 4a, red and blue lines, respectively) were successfully reproduced in calculated CD spectra obtained with the use of time-dependent (TD) DFT (Fig. 4b, red and blue lines, respectively), from the structures of  $2\text{Th-L}^R\cdot\text{L}^R$  optimized with *P*-helicity and  $2\text{Th-L}^S\cdot\text{L}^S$  optimized with *M*-helicity (Fig. 4b, inset). The TD DFT calculation suggested that electronic transition corresponding to the first cotton band (excited state 1) arises from molecular orbitals along with the three bridged bis-diketone ligands (Fig. 4c), indicating that the origin of the biphasic CD spectra is excitonic splitting inside the helicates.<sup>18</sup> The helix sense of the other helicates was determined in the same manner (Fig. S10–S12†), to reveal that both  $2\text{Th}$  and  $3\text{Th}$  favor *P*-helicity with *R* guest co-ligands ( $\text{L}^R$  and  $\text{L}'^R$ ), and *M*-helicity with *S* guest co-ligands ( $\text{L}^S$  and  $\text{L}'^S$ ). The DFT calculations also indicated that *M*- $2\text{Th-L}^S\cdot\text{L}^S$  and *P*- $2\text{Th-L}^R\cdot\text{L}^R$  are  $12.33\text{ kcal mol}^{-1}$  lower in energy than that of *P*- $2\text{Th-L}^S\cdot\text{L}^S$  and *M*- $2\text{Th-L}^R\cdot\text{L}^R$  (diastereomers), respectively (Fig. 5a). The *M*- $2\text{Th-L}^S\cdot\text{L}^S$  and *P*- $2\text{Th-L}^R\cdot\text{L}^R$  have two ligand-to-ligand interactions ( $\pi$ - $\pi$  interactions) with the guest co-ligands, while *P*- $2\text{Th-L}^S\cdot\text{L}^S$  and *M*- $2\text{Th-L}^R\cdot\text{L}^R$  (diastereomers) contain only one ligand-to-ligand interaction inside the assembly (Fig. 5a). In the same manner, the optimized structures of *M*- $2\text{Th-L}^S\cdot\text{L}^S$  and *P*- $2\text{Th-L}^R\cdot\text{L}^R$  are  $7.44\text{ kcal mol}^{-1}$  lower in energy than that of *P*- $2\text{Th-L}^S\cdot\text{L}^S$  and *M*- $2\text{Th-L}^R\cdot\text{L}^R$  (diastereomers), respectively (Fig. 5b). These DFT results can explain the fact that  $2\text{Th}$  favored *P*-helicity with the *R*-guest co-ligands ( $\text{L}^R$  and  $\text{L}'^R$ ), and *M*-helicity with the *S*-guest co-ligands ( $\text{L}^S$  and  $\text{L}'^S$ ). More importantly, the DFT calculations predict that homochiral assemblies ( $2\text{Th-L}^R\cdot\text{L}^R$ ,  $2\text{Th-L}^S\cdot\text{L}^S$ ,  $2\text{Th-L}^R\cdot\text{L}'^R$ , and  $2\text{Th-L}^S\cdot\text{L}'^S$ ) are  $5.99$ – $7.00\text{ kcal mol}^{-1}$  lower in energy than that of heterochiral assemblies ( $2\text{Th-L}^R\cdot\text{L}^S$  and  $2\text{Th-L}^R\cdot\text{L}'^S$ ) [Fig. 5a and b].<sup>28</sup> Additionally, the DFT calculations provide an important prediction concerning on the performed complexes (1 : 1 complexes): even the initial terminal binding of the chiral guest co-ligands will induce the helical conformation of  $2\text{Th}$  and  $3\text{Th}$ , where the *M*-helix structures (1 : 1 complexes) with the *S*-guest co-ligands ( $\text{L}^S$  and  $\text{L}'^S$ ) are  $4.16$ – $6.45\text{ kcal mol}^{-1}$  lower in energy than that of the *P*-helix structures (Fig. 5c) as in the case of the final assemblies (1 : 2 complexes).



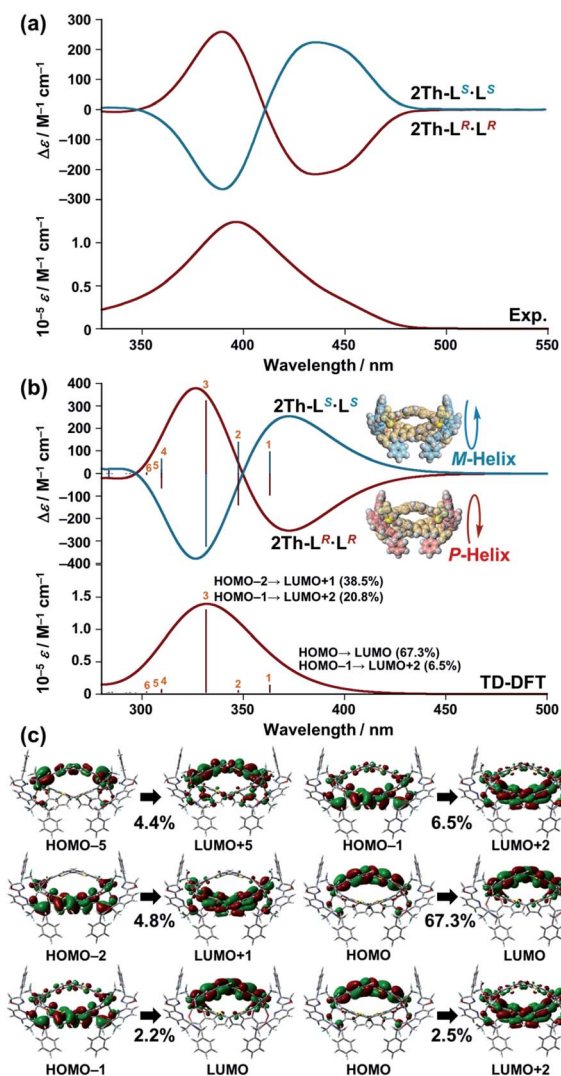


Fig. 4 (a) Experimentally obtained UV-vis and CD spectra of 2Th- $L^R.L^R$  (red line) and 2Th- $L^S.L^S$  (blue line) in acetone. (b) Theoretical CD spectrum [time dependent-DFT/CAM-B3LYP-6-31G(d) [C H N O S F]/LANL2DZ (Sc)] of the optimized structure [DFT/CAM-B3LYP-6-31G(d) [C H N O S F]/LANL2DZ (Sc)] of  $P$ -2Th- $L^R.L^R$  and  $M$ -2Th- $L^S.L^S$ , where Eu atoms are replaced by Sc atoms to reduce the calculation complexity (Fig. S10–S12†). (c) Summary of excited state 1.

### Helix length-dependent over 1 nm-range chirality recognition

On the basis of these results, we investigated the effects of the helix length on the long-range chirality recognition by monitoring the induced CD signals of **2Th** and **3Th** ( $d_{L_n-L_n} = 11.5$  and  $14.0$  Å, respectively) on changing the enantiomeric excess (ee) of the chiral guest co-ligands in the range from  $ee = ([R] - [S])/([R] + [S]) = 0$  to  $+1$  and to  $-1$  (Fig. 6 left, red and blue lines, respectively). Here, the total concentration of chiral ligands  $[R] + [S]$  remained constant at each molar ratio, *ca.* a 90-fold excess against **2Th** and **3Th**. Such excess conditions are required for a clear distinguishment on whether the plot of  $\Delta\epsilon$  versus ee (Fig. 6 right) follows the positive nonlinear (sigmoidal) or linear relationship (*vide infra*). A positive nonlinear relationship was clearly observed for the combination of **2Th** with  $L^R$  and  $L^S$

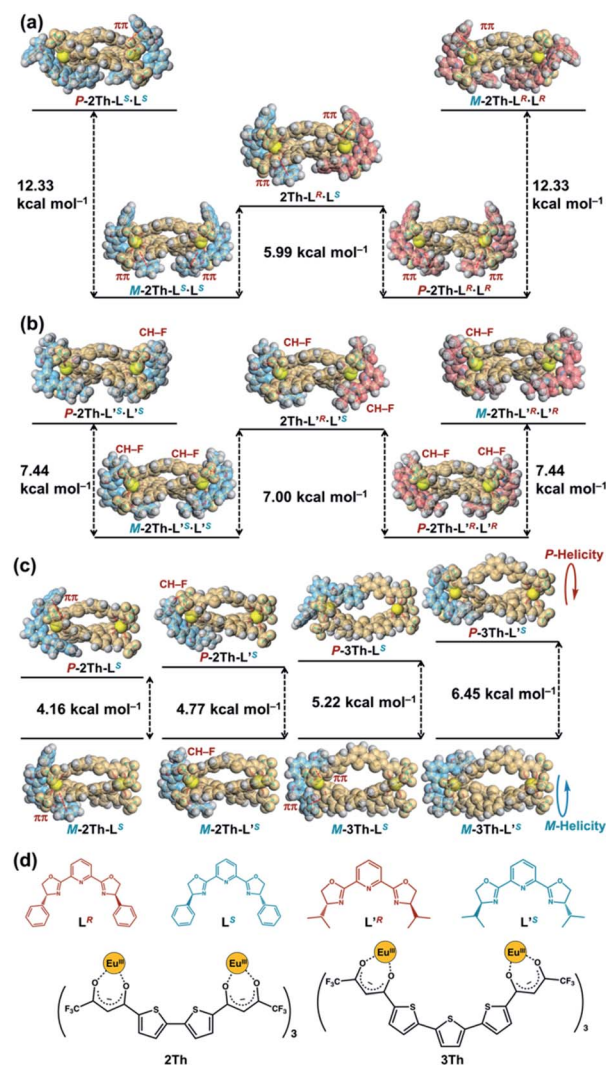


Fig. 5 Relative energy difference between the optimized structures of (a)  $P$ -2Th- $L^S.L^S$ ,  $M$ -2Th- $L^S.L^S$ , 2Th- $L^R.L^S$ ,  $P$ -2Th- $L^R.L^R$ , and  $M$ -2Th- $L^R.L^R$ , (b)  $P$ -2Th- $L^S.L^S$ ,  $M$ -2Th- $L^S.L^S$ , 2Th- $L^R.L^S$ ,  $P$ -2Th- $L^R.L^R$ , and  $M$ -2Th- $L^R.L^R$ , (c)  $M$ -2Th- $L^S$  and  $P$ -2Th- $L^S$ ,  $M$ -2Th- $L^S$  and  $P$ -2Th- $L^S$ ,  $M$ -3Th- $L^S$  and  $P$ -3Th- $L^S$ ,  $M$ -3Th- $L^S$  and  $P$ -3Th- $L^S$  [DFT/CAM-B3LYP/def2SVP (C H N O S F)/def2TZVP (La)], where the Eu atoms were replaced by La atoms. (d) Chemical structures of  $L^R$ ,  $L^S$ ,  $L^R$ ,  $L^S$ , **2Th**, and **3Th**.

(Fig. 6a, right). The experimentally obtained nonlinear relationship is explained by eqn (1) derived from Scheme 3a (Appendix 1†):

$$\Delta\epsilon/\Delta\epsilon_\infty = 4ee(K_{RR}/K_{(\text{hetero})})/(2(1 + ee^2) + (K_{RR}/K_{(\text{hetero})}) + (1 - ee^2)) \quad (1)$$

where  $\Delta\epsilon_\infty$  denotes the  $\Delta\epsilon$  value of the homochiral assemblies at  $ee = +1$ . A positive nonlinear relationship is expected when the system follows chiral-self recognition because  $K_{RR}/K_{(\text{hetero})} > 0.50$ , and the degree of sigmoidal character increases together with the  $K_{RR}/K_{(\text{hetero})}$  value (here,  $K_{(\text{hetero})} = K_{RS} + K_{SR} = 2K_{RS} = 2K_{SR}$ ).<sup>29,30</sup> The observed positive nonlinear relationship (Fig. 6a, right) agreed well with the calculated curve with  $K_{RR}/K_{(\text{hetero})} =$



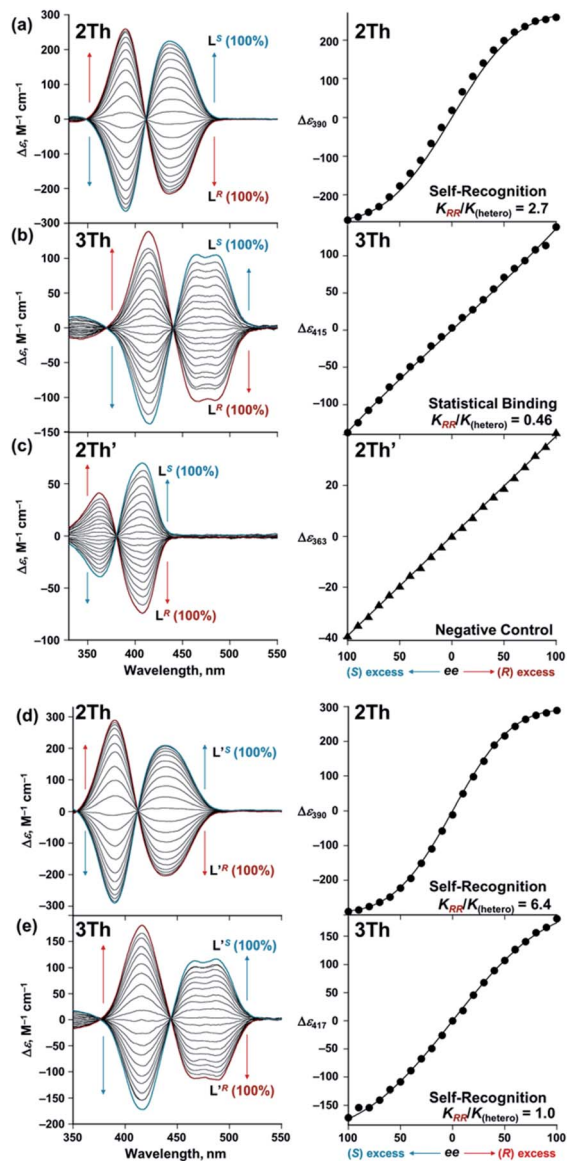
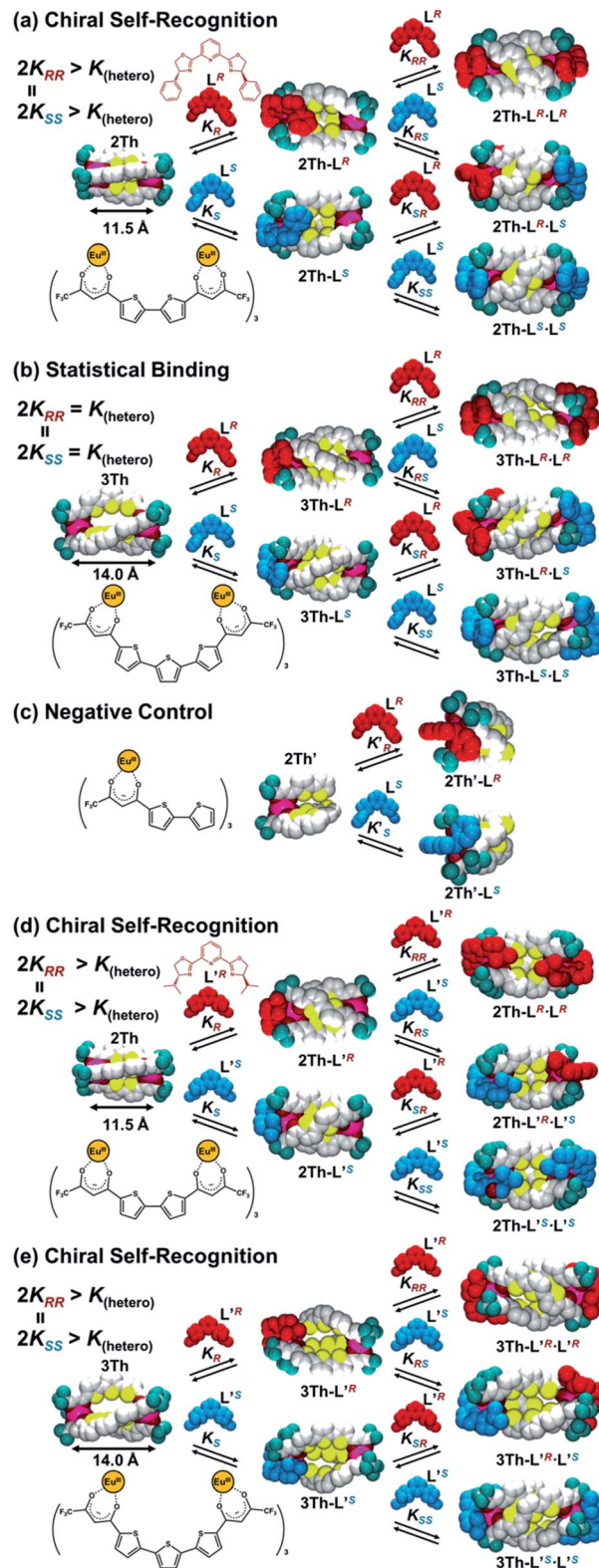


Fig. 6 Left: CD spectra of (a) and (d) 2Th ( $7.2 \times 10^{-6}$  M), (b) and (e) 3Th ( $5.3 \times 10^{-6}$  M), and (c) 2Th' ( $9.4 \times 10^{-6}$  M) in the presence of different enantiomeric excess (ee) of  $L^{(R \text{ or } S)}$  [total concentrations: (a)  $6.6 \times 10^{-4}$  M, (b)  $4.9 \times 10^{-4}$  M, (c)  $8.7 \times 10^{-4}$  M],  $L^{(R \text{ or } S)}$  [total concentrations: (d)  $7.5 \times 10^{-4}$  M and (e)  $5.1 \times 10^{-4}$  M] in acetone at 298 K. Right: plots of  $\Delta\epsilon$  versus ee of (a)–(c)  $L^{(R \text{ or } S)}$ , (d) and (e)  $L^{(R \text{ or } S)}$ .

2.7, with the use of eqn (1). Therefore, chiral self-recognition occurred in the self-assembly process of 2Th with  $L^R$  and  $L^S$  (Scheme 3a). The larger  $K_{RR}$  value than that of  $K_{RS}$  suggested a higher thermodynamic stability of the homochiral 2Th- $L^R \cdot L^R$  over the heterochiral 2Th- $L^R \cdot L^S$ , which is consistent with the above energy estimation from their DFT-optimized structures ( $\Delta E = 5.99 \text{ kcal mol}^{-1}$ , Fig. 5a). Notably, the degree of chiral self-recognition is highly temperature dependent. Whereas a high  $K_{RR}/K_{(hetero)}$  value was obtained at lower temperature,  $K_{RR}/K_{(hetero)} = 2.4$  at 323 K, 2.7 at 298 K, and 7.0 at 273 K (Table 2 and Fig. S15<sup>†</sup>). This trend implies a major role of the enthalpy term in the chiral-self-recognition nature, which likely arises from



Scheme 3 Summary of self-sorting for  $L^R$  and  $L^S$  with (a) 2Th, (b) 3Th, (c) 2Th', and those for  $L^{(R)}$  and  $L^{(S)}$  with (d) 2Th and (e) 3Th, where  $K_{(hetero)} = K_{RS} + K_{SR} = 2K_{RS} = 2K_{SR}$ .

ligand-to-ligand interactions between 2Th and  $L^R$  or  $L^S$  (*vide supra*, Fig. 1b). Conversely, 3Th with a longer helix length ( $d_{Ln-Ln} = 14.0 \text{ \AA}$ ) had an almost completely linear relationship



**Table 2** Ratios of binding constants ( $K_{RR}/K_{(\text{hetero})}$ ) in self-assembly formation of **2Th** and **3Th** with chiral guest co-ligands, where  $K_{(\text{hetero})} = K_{RS} + K_{SR} = 2K_{RS} = 2K_{SR}$

Guest co-ligand	<b>2Th</b> $K_{RR}/K_{(\text{hetero})}$			<b>3Th</b> $K_{RR}/K_{(\text{hetero})}$		
	323 K	298 K	273 K	323 K	298 K	273 K
R = Ph ( $L^R$ , $L^S$ )	2.4	2.7	7.0	0.70	0.46	0.56
R = <sup>i</sup> Pr ( $L^R$ , $L^S$ )	4.6	6.4	>10.0	0.90	1.00	1.05

between  $\Delta\epsilon$  and ee in their self-assembly process with  $L^R$  and  $L^S$  (Fig. 6b, right). The linear relationship between  $\Delta\epsilon$  and ee can be described by eqn (1) with  $K_{RR}/K_{(\text{hetero})} = 0.46$ , suggesting statistical binding of  $L^R$  and  $L^S$  to **3Th** (Scheme 3b). The value of  $K_{RR}/K_{(\text{hetero})} = 0.46$  indicates that homochiral (**3Th**- $L^R \cdot L^R$  and **3Th**- $L^S \cdot L^S$ ) and heterochiral assemblies (**3Th**- $L^R \cdot L^S$ ) have almost the same thermodynamic stability, which is likely attributed to the longer thiophene spacer units of **3Th** that create flexibility in the helix chain and prohibit effective chirality information transfer.<sup>28</sup> Hence, the value of  $K_{RR}/K_{(\text{hetero})}$  in self-assembly of **3Th** with  $L^R$  and  $L^S$  was almost temperature independent (Table 2 and Fig. S16<sup>†</sup>). Conversely, a complete linear relationship was successfully obtained between  $\Delta\epsilon$  and ee during the self-assembly of mononuclear complex **2Th'** with  $L^R$  and  $L^S$  (Fig. 6c, right), where **2Th'** exhibited induced biphasic CD signals (Fig. 6c, left) similar to the case of the dinuclear helicates (**2Th** and **3Th**). Therefore, the negative control experiments revealed that even the initial terminal binding of  $L^R$  or  $L^S$  to **2Th** induced helicate structures prior to the final assembly (Scheme 3), which is also in good agreement with the DFT prediction (Fig. 5c, *vide supra*). Conversely, when the phenyl groups of  $L^R$  and  $L^S$  were replaced by isopropyl groups ( $L^R$  and  $L^S$ , respectively), a higher degree of chiral self-recognition was achieved by a combination of **2Th** with  $L^R$  and  $L^S$  in terms of a higher value of  $K_{RR}/K_{(\text{hetero})}$  (2.7  $\rightarrow$  6.4, Fig. 6d and Table 1), where the chiral self-recognition feature was maximized at 273 K ( $K_{RR}/K_{(\text{hetero})} > 10.0$ , Fig. S15<sup>†</sup> and Table 2). The above DFT calculations indicate that homochiral **2Th**- $L^S \cdot L^S$  is 7.00 kcal mol<sup>-1</sup> lower in energy than that of heterochiral **2Th**- $L^R \cdot L^S$  (Fig. 5b), which was larger than that between **2Th**- $L^S \cdot L^S$  and **2Th**- $L^R \cdot L^S$  (5.99 kcal mol<sup>-1</sup>, Fig. 5a). Notably, a plot of  $\Delta\epsilon$  versus ee obtained in combination of **3Th** with  $L^R$  and  $L^S$  suggested  $K_{RR}/K_{(\text{hetero})} = 1.0$  (Fig. 6e), indicating that chiral self-recognition can be achieved even for **3Th** with longer helix lengths (Scheme 3e and Fig. S17–S19<sup>†</sup>).

Finally, conclusive evidence for the chiral self-recognition versus statistical binding mechanism was obtained by <sup>19</sup>F NMR measured under enantiopure and racemic conditions of the chiral guest co-ligands (Fig. 7). Under the racemic conditions ( $[\mathbf{3Th}] : [L^R] : [L^S] = 1 : 1 : 1$ ), the <sup>19</sup>F NMR spectrum of **3Th** (Fig. 7b) had new signals (purple squares) other than those corresponding to the homochiral assemblies (**3Th**- $L^R \cdot L^R$  and **3Th**- $L^S \cdot L^S$ , red and blue circles) observed under the enantiopure conditions ( $[\mathbf{3Th}] : [L^R] : [L^S] = 1 : 2 : 0$ , Fig. 7c). Hence, the new

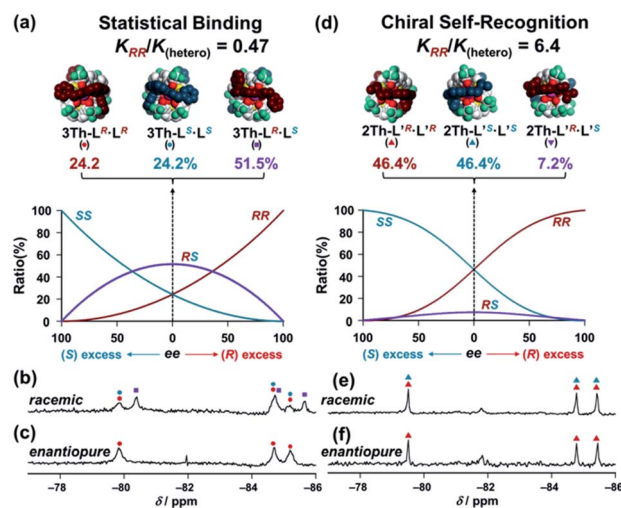


**Fig. 7** Theoretical product ratio at ee = 0 between (a) **3Th**- $L^R \cdot L^R$  (red) and **3Th**- $L^S \cdot L^S$  (blue) and **3Th**- $L^R \cdot L^S$  (purple) calculated based on eqn (1) with  $K_{RR}/K_{(\text{hetero})} = 0.47$ , (d) **2Th**- $L^R \cdot L^R$  (red) and **2Th**- $L^S \cdot L^S$  (blue) and **2Th**- $L^R \cdot L^S$  (purple) calculated based on eqn (1) with  $K_{RR}/K_{(\text{hetero})} = 6.4$ , where  $K_{(\text{hetero})} = K_{RS} + K_{SR} = 2K_{RS} = 2K_{SR}$ . <sup>19</sup>F NMR spectra of **3Th** under the (b) racemic conditions [**3Th**] : [ $L^R$ ] : [ $L^S$ ] = 1 : 1 : 1, (c) enantiopure conditions [**3Th**] : [ $L^R$ ] : [ $L^S$ ] = 1 : 2 : 0, those of **2Th** under the (e) racemic conditions [**2Th**] : [ $L^R$ ] : [ $L^S$ ] = 1 : 1 : 1, (f) enantiopure conditions [**2Th**] : [ $L^R$ ] : [ $L^S$ ] = 1 : 2 : 0, in acetone-*d*<sub>6</sub> at 298 K. Symbols correspond to those for the structures of (a) and (d), red circles: **3Th**- $L^R \cdot L^R$ , blue circles: **3Th**- $L^S \cdot L^S$ , purple squares: **3Th**- $L^R \cdot L^S$ , red triangles: **2Th**- $L^R \cdot L^R$ , blue triangles: **2Th**- $L^S \cdot L^S$ .

signals (Fig. 7b, purple squares) are responsible for the heterochiral assembly (**3Th**- $L^R \cdot L^S$ ) formed under the racemic conditions. The ratio between the homochiral and heterochiral assemblies was determined to be [**3Th**- $L^R \cdot L^R$  + **3Th**- $L^S \cdot L^S$ ] : [**3Th**- $L^R \cdot L^S$ ] = 1.0 : 1.2 from the integrated ratio of the <sup>19</sup>F NMR signals, which agreed well with the theoretical product ratio at ee = 0 calculated from  $K_{RR}/K_{(\text{hetero})} = 0.46$  (Fig. 7a). This assignment is consistent with the statistical binding mechanism for a self-assembly process of **3Th** with  $L^R$  and  $L^S$  (Scheme 3b). Conversely, the <sup>19</sup>F NMR spectrum of **2Th** measured under racemic conditions ( $[\mathbf{2Th}] : [L^R] : [L^S] = 1 : 1 : 1$ , Fig. 7e) was identical to that obtained under the enantiopure conditions ( $[\mathbf{2Th}] : [L^R] : [L^S] = 1 : 2 : 0$ , Fig. 7f). The theoretical product ratio between homochiral and heterochiral assemblies is [**2Th**- $L^R \cdot L^R$  + **2Th**- $L^S \cdot L^S$ ] : [**2Th**- $L^R \cdot L^S$ ] = 92.8 : 7.2 (at ee = 0) calculated from  $K_{RR}/K_{(\text{hetero})} = 6.4$  (Fig. 4d),<sup>31</sup> which also underlines the strong chiral self-recognition behavior for self-assembly of **2Th** with  $L^R$  and  $L^S$  (Scheme 3d).

## Conclusions

In conclusion, we successfully demonstrated that helix chain (mediator) length can control when long-range chiral recognition occurs through chiral self-recognition or in statistical manner. Self-assembly of the shorter helicate **2Th** ( $d_{\text{Ln-Ln}} = 11.5$  Å) with chiral guest co-ligands ( $L^R$  and  $L^S$ ) resulted in chiral self-recognition (Scheme 3a), forming mainly homochiral assemblies (**2Th**- $L^R \cdot L^R$  and **2Th**- $L^S \cdot L^S$ ) rather than heterochiral



assemblies ( $2\text{Th-L}^R\cdot\text{L}^S$ ). Conversely, self-assembly of the longer helicate  $3\text{Th}$  ( $d_{\text{Ln-Ln}} = 14.0 \text{ \AA}$ ) with  $\text{L}^R$  and  $\text{L}^S$  occurred in a statistical binding manner (Scheme 3b), resulting in formation of the heterochiral ( $3\text{Th-L}^R\cdot\text{L}^S$ ) and homochiral assemblies ( $3\text{Th-L}^R\cdot\text{L}^R$  and  $3\text{Th-L}^S\cdot\text{L}^S$ ) in an almost 1 : 1 ratio. Subtle modification on the side arms of the chiral guest co-ligands ( $\text{L}^{(R \text{ or } S)} \rightarrow \text{L}^{(R \text{ or } S)}$ ) enables even the longer helicate  $3\text{Th}$  to achieve over 1.4 nm-range chirality recognition (Scheme 3e). Thus, the present findings open up opportunities for rational planning of molecular communication through the use of chirality as simple chemical input across long distances.

## Author contributions

N. S., H. I., and N. O. performed the synthesis and characterization of materials, and also contributed the titration experiments. Y. O. contributed the analysis of the X-ray crystal structure. J. Y. designed the study, analysed the experimental data and wrote the manuscript.

## Conflicts of interest

There are no conflicts to declare.

## Acknowledgements

This work was partly supported by JSPS KAKENHI Grant Numbers JP19H02693, JP19K22207, and JP19H04596 in Scientific Research on Innovative Areas "Coordination Asymmetry", Grant-in-Aid for the ASAHI Glass Foundation. We thank the Edanz Group ([www.edanzediting.com/ac](http://www.edanzediting.com/ac)) for editing a draft of this manuscript.

## Notes and references

- G. Cooke and V. M. Rotello, *Chem. Soc. Rev.*, 2002, **31**, 275.
- L.-J. Chen, H.-B. Yang and M. Shionoya, *Chem. Soc. Rev.*, 2017, **46**, 2555.
- (a) M. Liu, L. Zhang and T. Wang, *Chem. Rev.*, 2015, **115**, 7304; (b) H. Jędrzejewska and A. Szumna, *Chem. Rev.*, 2017, **117**, 4863; (c) R. L. Greenaway, V. Santolini, A. Pulido, M. A. Little, B. M. Alston, M. E. Briggs, G. M. Day, A. I. Cooper and K. E. Jelfs, *Angew. Chem., Int. Ed.*, 2019, **58**, 16275; (d) M. M. Safont-Sempere, G. Fernández and F. Würthner, *Chem. Rev.*, 2011, **111**, 5784.
- (a) J. Zhong, L. Zhang, D. P. August, G. F. S. Whitehead and D. A. Leigh, *J. Am. Chem. Soc.*, 2019, **141**, 14249; (b) S. Kai, T. Kojima, F. L. Thorp-Greenwood, M. J. Hardie and S. Hiraoka, *Chem. Sci.*, 2018, **9**, 4104; (c) E. Chinnaraja, R. Arunachalam, E. Suresh, S. K. Sen, R. Natarajan and P. S. Subramanian, *Inorg. Chem.*, 2019, **58**, 4465; (d) V. E. Pritchard, D. Rota Martir, S. Oldknow, S. Kai, S. Hiraoka, N. J. Cookson, E. Zysman-Colman and M. J. Hardie, *Chem.-Eur. J.*, 2017, **23**, 6290; (e) S. A. Boer and D. R. Turner, *Chem. Commun.*, 2015, **51**, 17375; (f) O. Gidron, M. Jirásek, N. Trapp, M. O. Ebert, X. Zhang and F. Diederich, *J. Am. Chem. Soc.*, 2015, **137**, 12502; (g) Y. Tsunoda, M. Takatsuka, R. Sekiya and T. Haino, *Angew. Chem., Int. Ed.*, 2017, **56**, 2613; (h) W. Naito, K. Urakawa, R. Sato, Y. Shigeta, N. Yasuda and H. Maeda, *Org. Biomol. Chem.*, 2019, **17**, 1163.
- (a) C. Kaes, M. W. Hosseini, C. E. F. Rickard, B. W. Skelton and A. H. White, *Angew. Chem., Int. Ed.*, 1998, **37**, 920; (b) M. A. Masood, E. J. Enemark and T. D. P. Stack, *Angew. Chem., Int. Ed.*, 1998, **37**, 928; (c) S. G. Telfer, T. Sato, R. Kuroda, J. Lefebvre and D. B. Leznoff, *Inorg. Chem.*, 2004, **43**, 421; (d) T. W. Kim, M. S. Lah and J.-I. Hong, *Chem. Commun.*, 2001, 743; (e) J. M. Rowland, M. M. Olmstead and P. K. Mascharak, *Inorg. Chem.*, 2002, **41**, 1545; (f) G. Zhang, G. Gil-Ramírez, A. Markevicius, C. Browne, I. J. Vitorica-Yrezabal and D. A. Leigh, *J. Am. Chem. Soc.*, 2015, **137**, 10437.
- (a) L. Volbach, N. Struch, F. Bohle, F. Topić, G. Schnakenburg, A. Schneider, K. Rissanen, S. Grimme and A. Lützen, *Chem.-Eur. J.*, 2020, **26**, 3335; (b) J. Anhäuser, R. Puttreddy, L. Glanz, A. Schneider, M. Engeser, K. Rissanen and A. Lützen, *Chem.-Eur. J.*, 2019, **25**, 12294; (c) T. R. Schulte, J. J. Holstein and G. H. Clever, *Angew. Chem., Int. Ed.*, 2019, **58**, 5562.
- (a) D. Beaudoin, F. Rominger and M. Mastalerz, *Angew. Chem., Int. Ed.*, 2017, **56**, 1244; (b) L. Y. Yao, T. K. M. Lee and V. W. W. Yam, *J. Am. Chem. Soc.*, 2016, **138**, 7260; (c) C. G. Claessens and T. Torres, *J. Am. Chem. Soc.*, 2002, **124**, 14522.
- (a) S. Iseki, K. Nonomura, S. Kishida, D. Ogata and J. Yuasa, *J. Am. Chem. Soc.*, 2020, **142**, 15842; (b) D. Ogata and J. Yuasa, *Chem. Commun.*, 2020, **56**, 8679; (c) K. Nonomura and J. Yuasa, *Inorg. Chem.*, 2019, **58**, 6474; (d) Y. Imai, Y. Nakano, T. Kawai and J. Yuasa, *Angew. Chem., Int. Ed.*, 2018, **57**, 8973; (e) Y. Imai and J. Yuasa, *Chem. Sci.*, 2019, **10**, 4236; (f) Y. Imai and J. Yuasa, *Chem. Commun.*, 2019, **55**, 4095; (g) D. Ogata and J. Yuasa, *Angew. Chem., Int. Ed.*, 2019, **58**, 18424.
- (a) L. L. Yan, C. H. Tan, G. L. Zhang, L. P. Zhou, J. C. Bünzli and Q. F. Sun, *J. Am. Chem. Soc.*, 2015, **137**, 8550; (b) Y. Zhou, H. Li, T. Zhu, T. Gao and P. Yan, *J. Am. Chem. Soc.*, 2019, **141**, 19634; (c) C.-T. Yeung, K.-H. Yim, H.-Y. Wong, R. Pal, W.-S. Lo, S.-C. Yan, M. Yee-Man Wong, D. Yufit, D. E. Smiles, L. J. McCormick, S. J. Teat, D. K. Shuh, W.-T. Wong and G.-L. Law, *Nat. Commun.*, 2017, **8**, 1128; (d) H.-Y. Wong, W.-S. Lo, K.-H. Yim and G.-L. Law, *Chem.*, 2019, **5**, 3058; (e) J. Lisowski, *Inorg. Chem.*, 2011, **50**, 5567; (f) M. Iwamura, M. Fujii, A. Yamada, H. Koike and K. Nozaki, *Chem.-Asian J.*, 2019, **14**, 561.
- E. Yashima, N. Ousaka, D. Taura, K. Shimomura, T. Ikai and K. Maeda, *Chem. Rev.*, 2016, **116**, 13752.
- (a) M. Albrecht, *Chem. Rev.*, 2001, **101**, 3457; (b) M. Boiocchi and L. Fabbrizzi, *Chem. Soc. Rev.*, 2014, **43**, 1835.
- D. E. Barry, D. F. Caffrey and T. Gunnlaugsson, *Chem. Soc. Rev.*, 2016, **45**, 3244.
- (a) J. Shi, Y. Hou, W. Chu, X. Shi, H. Gu, B. Wang and Z. Sun, *Inorg. Chem.*, 2013, **52**, 5013; (b) B. Li, H. Li, P. Chen, W. Sun, C. Wang, T. Gao and P. Yan, *Phys. Chem. Chem. Phys.*, 2015,





- 17, 30510; (c) B. Li, H. Li, P. Chen, W. Sun, C. Wang, T. Gao and P. Yan, *Dalton Trans.*, 2016, **45**, 11459.
- 14 B. El Aroussi, S. Zebret, C. Besnard, P. Perrottet and J. Hamacek, *J. Am. Chem. Soc.*, 2011, **133**, 10764.
- 15 (a) A. M. Johnson, M. C. Young, X. Zhang, R. R. Julian and R. J. Hooley, *J. Am. Chem. Soc.*, 2013, **135**, 17723; (b) A. M. Johnson, C. A. Wiley, M. C. Young, X. Zhang, Y. Lyon, R. R. Julian and R. J. Hooley, *Angew. Chem., Int. Ed.*, 2015, **54**, 5641.
- 16 (a) T. Lathion, L. Guénée, C. Besnard, A. Bousseksou and C. Piguet, *Chem.–Eur. J.*, 2018, **24**, 16873; (b) D. Zare, Y. Suffren, H. Nozary, A. Hauser and C. Piguet, *Angew. Chem., Int. Ed.*, 2017, **56**, 14612.
- 17 (a) Y. Zhou, Y. Yao, Z. Cheng, T. Gao, H. Li and P. Yan, *Inorg. Chem.*, 2020, **59**, 12850; (b) D. Liu, Y. Zhou, Y. Zhang, H. Li, P. Chen, W. Sun, T. Gao and P. Yan, *Inorg. Chem.*, 2018, **57**, 8332; (c) W. Chen, X. Tang, W. Dou, B. Wang, L. Guo, Z. Ju and W. Liu, *Chem.–Eur. J.*, 2017, **23**, 9804; (d) C.-T. Yeung, W. T. K. Chan, S.-C. Yan, K.-L. Yu, K.-H. Yim, W.-T. Wong and G.-L. Law, *Chem. Commun.*, 2015, **51**, 592.
- 18 (a) T. Y. Bing, T. Kawai and J. Yuasa, *J. Am. Chem. Soc.*, 2018, **140**, 3683; (b) J. Yuasa, T. Ohno, K. Miyata, H. Tsumatori, Y. Hasegawa and T. Kawai, *J. Am. Chem. Soc.*, 2011, **133**, 9892; (c) Y. Okayasu and J. Yuasa, *Mol. Syst. Des. Eng.*, 2018, **3**, 66; (d) Y. B. Tan, M. Yamada, S. Katao, Y. Nishikawa, F. Asanoma, J. Yuasa and T. Kawai, *Inorg. Chem.*, 2020, **59**, 12867; (e) Y. B. Tan, Y. Okayasu, S. Katao, Y. Nishikawa, F. Asanoma, M. Yamada, J. Yuasa and T. Kawai, *J. Am. Chem. Soc.*, 2020, **142**, 17653.
- 19 G. Desimoni, G. Faita and P. Quadrelli, *Chem. Rev.*, 2003, **103**, 3119.
- 20 A. de Bettencourt-Dias, P. S. Barber and S. Bauer, *J. Am. Chem. Soc.*, 2012, **134**, 6987.
- 21 M. Leonzio, A. Melchior, G. Faura, M. Tolazzi, F. Zinna, L. Di Bari and F. Piccinelli, *Inorg. Chem.*, 2017, **56**, 4413.
- 22 (a) R. Carr, N. H. Evans and D. Parker, *Chem. Soc. Rev.*, 2012, **41**, 7673; (b) G. Muller, *Dalton Trans.*, 2009, 9692–9707; (c) D. Parker, R. S. Dickins, H. Puschmann, C. Crossland and J. A. K. Howard, *Chem. Rev.*, 2002, **102**, 1977; (d) C. M. G. dos Santos, A. J. Harte, S. J. Quinn and T. Gunnlaugsson, *Coord. Chem. Rev.*, 2008, **252**, 2512; (e) J.-C. G. Bünzli and C. Piguet, *Chem. Soc. Rev.*, 2005, **34**, 1048; (f) F. Zinna and L. Di Bari, *Chirality*, 2015, **27**, 1.
- 23 J. M. Dragna, G. Pescitelli, L. Tran, V. M. Lynch, E. V. Anslyn and L. Di Bari, *J. Am. Chem. Soc.*, 2012, **134**, 4398.
- 24 S. P. Morcillo, D. Miguel, L. Á. de Cienfuegos, J. Justicia, S. Abbate, E. Castiglioni, C. Bour, M. Ribagorda, D. J. Cárdenas, J. M. Paredes, L. Crovetto, D. Choquesillo-Lazarte, A. J. Mota, M. C. Carreño, G. Longhi and J. M. Cuerva, *Chem. Sci.*, 2016, **7**, 5663.
- 25 The negative charge may come from reduction of Eu<sup>III</sup> or the bis-diketone ligand having thiophene spacers during the ionization process of mass.
- 26 (a) L. Babel, T. N. Y. Hoang, L. Guénée, C. Besnard, T. A. Wesolowski, M. Humbert-Droz and C. Piguet, *Chem.–Eur. J.*, 2016, **22**, 8113; (b) A. Zaïm, H. Nozary, L. Guénée, C. Besnard, J.-F. Lemonnier, S. Petoud and C. Piguet, *Chem.–Eur. J.*, 2012, **18**, 7155.
- 27 The small <sup>19</sup>F signals should be ascribed to a minor complex (e.g., coordination isomer) or the minor contribution of 2Th-L<sup>R</sup>.
- 28 Number of atoms in the 3Th-assemblies is too large to perform frequency calculation required for the zero point energy correction, and therefore the energy estimation of the assemblies of the 3Th-assemblies could not be accomplished in this study (Fig. S13 and S14†).
- 29 (a) D. Guillaneux, S.-H. Zhao, O. Samuel, D. Rainford and H. B. Kagan, *J. Am. Chem. Soc.*, 1994, **116**, 9430; (b) T. Satyanarayana, S. Abraham and H. B. Kagan, *Angew. Chem., Int. Ed.*, 2009, **48**, 456.
- 30 Self-recognition and self-discrimination was distinguished by whether the  $K_{RR}$  (or  $K_{SS}$ ) values are the half of the  $K_{(hetero)}$  value.
- 31 <sup>19</sup>F NMR signals due to the heterochiral assembly (2Th-L<sup>R</sup>·L<sup>S</sup>) should be less than detection level.

